Model for the emission of Si^+ ions during oxygen bombardment of Si(100) surfaces

J. L. Alay
Interuniversity Micro-Electronics Center, Kapeldreef 75, B-3001 Leuven, Belgium
and Facultat de Física, Universitat de Barcelona, Avgda. Diagonal 645-647, E-08028 Barcelona, Catalonia, Spain

W. Vandervorst
Interuniversity Micro-Electronics Center, Kapeldreef 75, B-3001 Leuven, Belgium
(Received 15 February 1994)

The variation in the emission of Si^+ ions from ion-beam-induced oxidized silicon surfaces has been studied. The stoichiometry and the electronic structure of the altered layer has been characterized using x-ray photoelectron spectroscopy (XPS). The XPS analysis of the Si 2*p* core level indicates the strong presence of suboxide chemical states when bombarding at angles of incidence larger than 30°. Since the surface stoichiometry or degree of oxidation varies with the angle of incidence, the corresponding valence-band structures also differ among each other. A comparison between experimental measurements and theoretically calculated Si and SiO_2 valence bands indicates that the valence bands for the altered layers are formed by a combination of those two. Since Si-Si bonds are present in the suboxide molecules, the top of the respective new valence bands are formed by the corresponding 3*p*-3*p* Si-like subbands, which extend up to the Si Fermi level. The changes in stoichiometry and electronic structure have been correlated with the emission of Si^+ ions from these surfaces. From the results a general model for the Si^+ ion emission is proposed combining the resonant tunneling and local-bond-breaking models.

I. INTRODUCTION

Despite all the efforts in trying to establish a global model for the emission of ions during low-energy sputtering, one cannot yet obtain a general description of the process, especially for the case of Si^+ ion emission.

Two different ionization mechanisms during sputtering have been proposed. On the one hand, the electron tunneling model[1–4] and on the other hand, the local-bond-breaking model.[4–8] Both models intend to explain the electronic changes undergone by an atom sputtered by ion bombardment of the target surface. An accurate description of these changes would give rise to a better quantification of ion yields in techniques such as secondary ion mass spectrometry (SIMS) and atomic surface scattering.

The electron tunneling effect has been tested in metals with much success. In this model and for the case of positive ion emission, the first ionization potential (I_p) plays a major role. For the case of a positive ion leaving the sample surface, owing to the screening by the electrons in the metal conduction band, the first ionization level [$i_p(z)$] is shifted up by an image potential inversely proportional to the distance ion-image plane (z) with respect to the value in the free space (the maximum shift takes place at distance zero, while for very large distance $i_p(\infty)=I_p$). While the sputtered ion leaves the surface there exists the possibility that the energy of the first ionization level coincides with the energy of occupied electronic levels (below the Fermi energy), and in this case, resonant electron tunneling is expected between the outgoing ion and the target surface, and hence neutralization of the outgoing ion can occur (see Fig. 1).

The ionization probability taking into account that effect can be calculated from first principles.[9–12] For a metal, the ionization probability for an atom sputtered from the surface, when the first ionization level [$i_p(z)$] is crossing the Fermi level, is given by

$$P^+ \approx \exp[-(I_p-\Phi)/\varepsilon_0] , \quad (1)$$

where the parameter ε_0 is proportional to the escaping velocity of the ion[12] and Φ is the work function. This expression is in good agreement with some experimental results (as in the case of chemisorbed Cs on metal surfaces).

The local-bond-breaking model, on the other hand, has

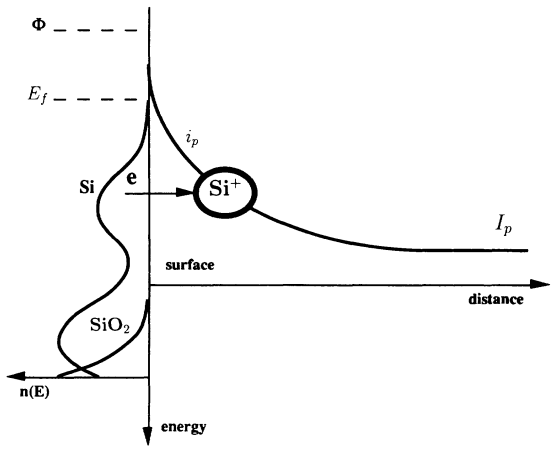

FIG. 1. Schematic energy diagram of an ion leaving a Si surface. The electron can tunnel between the electronic levels below the Fermi level (E_f) and the first ionization level (i_p) when they have the same energy.

been proposed in view of the chemical enhancement of the secondary ion emission as observed during oxygen bombardment and is applied to ionic and partially ionic materials (oxides). According to the Landau-Zener theory,[13–16] the anion left in a surface site can trap an electron from the outgoing atom when the covalent and ionic curves for the original molecule cross at a certain distance from the equilibrium position. Hence the ion yield will be related with the breaking of oxygen bonds locally. Instead of changes in global surface properties like band gap, the emission mechanism would be governed by the local molecular structure implying that the degree of oxidation would be a relevant parameter, since this will increase the probability of ion formation following the Landau-Zener theory.

Although both models have already been discussed at length in the literature, no detailed study is available that correlates in detail the observed mechanisms in Si^+ emission with changes in oxygen content and degree of oxidation. For instance the experiments carried out so far have never included a specific study of both photoelectron regions, Si $2p$ and the valence band. For oxygen-bombarded targets only partial studies[17,18] correlate the Si^+ signal with the O $1s$ signal measured by x-ray photoelectron spectroscopy (XPS), but only for very small coverages induced by thermal oxidation,[19] and not by oxygen bombardment. For low oxygen concentrations ($c < 35$ at. %). Wittmaack established a relation between Si^+ yields and oxygen concentration.

It is the purpose of the present paper to establish such a correlation over a wide range of oxygen concentration and to use information from the valence band as well as from the Si $2p$ regions to quantify the contribution from the different mechanisms. The angle of incidence of the primary beam is hereby used to control the oxygen concentration and the degree of oxidation in a reproducible manner.

In the first part of this paper, an *in-situ* XPS analysis of ion bombarded silicon surfaces is presented whereby the valence band as well as the Si $2p$ region are analyzed in detail. Since it is the first time to our knowledge that a study on the valence band for altered layers is described, special attention is paid to the XPS analysis of this region including a detailed comparison with the two available reference valence bands corresponding to Si and SiO_2.

In the second part of the paper, a general model, combining resonant tunneling and local bond breaking, for the atomic emission of Si^+ ions from ion induced oxidized Si(100) surfaces is proposed. Whilst the valence band photoemission variations reflect modifications on the electronic properties of the altered layer such as the band gap or the electronic structure, the variations on the Si $2p$ core level can be more easily correlated with localized bond changes. Hence the valence-band information can be used within the concept of the resonant tunneling model, whereas, the Si $2p$ core-level variations fit within the local-bond-breaking model.

II. EXPERIMENT

The Si(100) samples were bombarded with a 5-keV O_2^+ ion beam at angles of incidence of 0°, 15°, 25°, 30°, and 35°, with respect to the target normal, while rastering over 4×4 mm^2. *In-situ* XPS measurements were performed in the center of the rastered area, using a SSX-100 instrument. The base pressure of the analysis chamber is in the 10^{-10} Torr range and rises to 10^{-8} Torr during bombardment. All the samples showed a native oxide before bombardment no thicker than 20 nm as determined with angle-resolved XPS.

The ion-beam-induced oxidation of Si targets leads, in some cases, to the formation of several mixed different chemical bonds of Si atoms with other Si and/or O atoms. For instance, states corresponding to pure silicon, suboxides, and stoichiometric silicon oxide, all can be observed in the binding energy band from 99.0 to 105.0 eV approximately. The different oxidation states were derived from the Si $2p$ photoelectron peak by performing a detailed peak fitting. The constraints used in the peak fitting were those proposed in Ref. 20. The pure silicon component, referred to as Si^0, is actually composed of two peaks corresponding to the spin-orbit splitting of the $2p$ energy level into the $2p_{3/2}$ and $2p_{1/2}$, which lie at 99.5 and 100.6 eV. The ratio between areas has been constrained to a value of 2. The spin-orbit splitting for the rest of the peaks in the Si $2p$ region cannot be resolved and consequently they are considered as single peaks. The suboxide states are bonded to 1, 2, or 3 oxygen atoms and are referred to as Si^{1+}, Si^{2+}, and Si^{3+} states, respectively. The separation between these peaks is 1.0, 1.7, and 2.6 eV, relative to Si^0. Finally, the silicon oxide chemical state, denoted as Si^{4+}, and bonded to four oxygen atoms is separated approximately 4.0 eV from the Si^0.

The XPS analysis and interpretation of the valence-band structure is described in the next section.

III. RESULTS AND DISCUSSION

A. Study of the valence band

The validity of the local-bond-breaking and tunneling models requires a detailed investigation of the changes undergone by the valence band after bombarding the targets. The investigation necessarily starts from an overview of the valence bands for pure Si and SiO_2 surfaces. The following paragraphs describe the study by XPS of the valence-band structure for both materials and links the results to the theoretical models which describe this energy region. Despite the nonexistence of a unique assignment of the several subbands present in the valence-band region, as calculated by theoretical models, still a rather good interpretation of the XPS spectra can be accomplished.

For the characterization of the Si valence band, a Si(100) surface was HF (0.5%) dipped during 5 min and immediately loaded in the XPS analysis chamber. A quick survey analysis of the surface showed an ultraclean surface with only traces of adsorbed C and O. The presence of H cannot be detected by XPS. The XPS analysis of the valence band (binding energy between 0 and 20 eV referred to the Fermi energy of gold) was carried out with very high resolution over a period of four h, this in order to decrease the noise level due to the very low photoelec-

tron cross sections for valence-band electronic levels.

Before proceeding with the experimental results regarding the valence bands, it is worthwhile to take a close look at the theoretical predictions for these spectra. Several calculations have been made on the energy position of characteristic peaks of the density of states in the valence-band spectrum of crystalline Si and some of them are compared to experimental measurements.[21–34] In Table I we show the various peaks predicted by three of these models. The peak positions are labeled according to the characteristic symmetry or critical points of the band structure of Si (when spin-orbit interaction is not included) as a function of the wave vector.[21,22] The three models agree in a threefold structure, usually denoted as I, II, and III bands. The region I, with the lowest energy, can be associated mainly with *p-p* interactions (from Si 3*p* electrons), region II with *s-p* hybrids (Si 3*s*-Si 3*p* electrons) and finally region III with *s-s* interactions (Si 3*s* electrons).

In the same table the energy position of the different density-of-states features derived from XPS analysis of the valence band is shown as well. The agreement between experiment and calculations is striking and allows an accurate assignment of each of the peaks (region I: L_3, X_4, and $W_2+\Sigma_{1\,\min}$; region II: L_1 and W_1; region III: L_2 and Γ_1), and the valley between region I and II (V), which can be seen in Fig. 2. (Note that energy zero corresponds to the top of the valence band.) The feature W_2 cannot be experimentally separated from $\Sigma_{1\,\min}$, although the former is predicted by EPM (empirical pseudopotential method) and SCOPW (self-consistent orthogonal plane wave functions) calculations and the latter only by the calculations of Cohen *et al.* using a pseudopotential method.

It is also interesting to analyze the variations in valence-band features when the crystalline structure is lost either by preparing amorphous Si using evaporation[23] or by amorphization of crystalline Si using ion bombardment. The latter was performed in the XPS analysis chamber using an Ar^+ ion beam with low energy (2.5 keV). The valence band of the subsequent damaged Si matrix presents some differences with respect to crystalline Si and evaporated amorphous Si. Regions I and II, i.e., *p-p*, and *s-p* hybrid interactions, respectively, show lower intensity as compared to region III (*s-s* interactions) which becomes dominant. The *p*-like L_3 peak of region I has disappeared. For evaporated amorphous Si surfaces, regions II and III were found to merge in a single peak[23] at 8.5 eV, positioned between the L_1 and W_1 peaks found in crystalline Si.

TABLE I. Energies (eV) of the most significative features, i.e., peaks and valleys, in the crystalline-Si valence band derived from XPS analysis (±0.3 eV) and density-of-states calculations using different pseudopotentials. All energies were referenced to the top of the valence band (see Fig. 2).

Feature	XPS expt.	EPM[a]	SCOPW[b]	Cohen-Chelikowsky[c]
$L_{3(I)}$	1.6			1.2
$X_{4(I)}$	2.7	2.6	2.5	
$W_2, \Sigma_{1\min(I)}$	4.5,–	4.0,–	–,3.1	–,4.5
V	5.3	5.1	4.5	
$L_{1(II)}$	7.1	7.1	6.9	6.9
$W_{1(II)}$		8.2	8.2	
$L_{2(III)}$	9.8	10.0	9.6	9.5
$\Gamma_{1(III)}$	11.7	13.0	11.8	12.5

[a]References 23 and 24.
[b]References 23 and 25.
[c]Reference 21.

The achievement of a good understanding of the change in the valence for the altered layers starts with a reference to the case of perfect oxidation. In order to do that, a SiO_2 layer of 800 mn was thermally grown on a (100) Si substrate. The XPS analysis was performed following the same procedures as described above for the case of crystalline Si.

The various valence band and density-of-states calculations for SiO_2 materials show the presence of two well-defined valence-band structures: the lower valence bands and the upper valence bands.[35–47] The multiple assignment of peaks to these bands is based on the LCAO (linear combination of atomic orbitals) calculations made by Tossel *et al.*[46,47] for quartz which are applicable to amorphous SiO_2 as well, as shown in reflectivity spectra.[48] We have followed in our description of these bands the nomenclature given in those calculations. The lower valence bands extend from 16 eV to more than 25 eV and are almost solely formed by molecular orbitals ($4a_1$ and $3t_2$) with an O 2*s* nonbonding orbital origin, whereas the upper valence bands extend from the top of the valence band until 20 eV below it and show the most important bonding features. We have scanned the upper region, since our interest lies in the density of states closest to the top of the valence band.

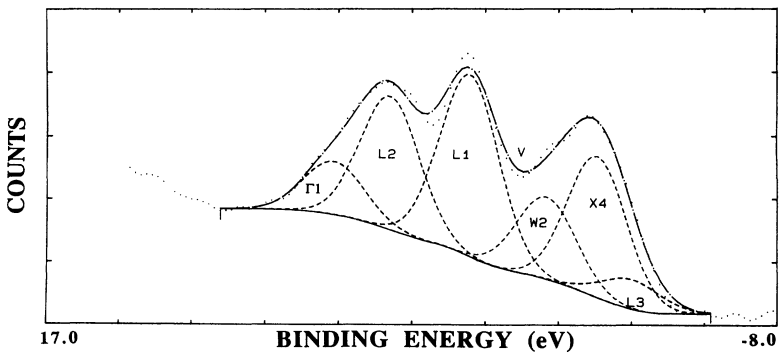

FIG. 2. XPS spectrum for the valence band of Si.

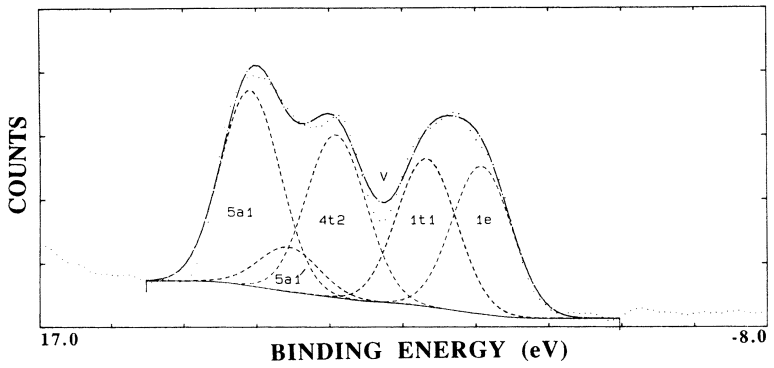

FIG. 3. XPS spectrum for the valence band of thermally grown SiO_2.

Theoretical calculations describe the upper valence bands as a group of several peaks distributed in two well-defined regions arising from very different orbital interactions between atoms: region I at the top of the valence-band side and region II at the "strongest bond" energy side. In Fig. 3, we show the corresponding XPS spectrum. (Note that the zero binding energy corresponds to the top of this valence band.)

Region II accounts for the Si-O bond occurring in a O-Si-O chain bent to an angle of about 150° for amorphous SiO_2. It is formed by two strong peaks and a very weak additional peak. The strong peaks correspond to $5a_1$ and $4t_2$ molecular orbitals arising from σ binding between the O $2p$ state and the Si $3s$ and Si $3p$ orbitals, respectively. Beside these two peaks we can resolve a third weak peak in between. This peak is not assigned in the calculations of Tossel *et al.* and we have called it $5a_1'$ (as a substructure of the $5a_1$ molecular orbital).

Region I is formed by the $1e$, $5t_2$, and $1t_1$ molecular orbitals, although the first two peaks are not resolved in the XPS spectra and form a single peak. The $5t_2$, $1e$, and $1t_1$ orbitals arise from nonbonding O $2p$ orbitals. The two components of O $2p$ nonbonding orbitals account for $2p$ orbitals perpendicular and parallel to the O-Si-O plane. Finally, a rather deep valley is also measured between region I and II (V).

Ultraviolet and photoemission spectroscopy and x-ray emission studies have corroborated these assignments.[35,49–51]

The energies of the various features determined in the valence band for SiO_2 are shown in Table II together with the assignment given by Fischer *et al.*[35] and the theoretical calculations of Tossel *et al.*,[46,47] and the corresponding XPS spectrum is shown in Fig. 3.

Once the valence band for Si and SiO_2 has been characterized in detail, we can investigate the valence bands for the surface of the altered layers, induced by ion-beam oxidation. Measurements were carried out for varying degrees of oxidation by using an energy of 5 keV at different angles of incidence corresponding to the transition region (35°–30°) and to the high oxidation region (30°–0°). For each experimental conditions, the incident oxygen dose was high enough such that stationary state was achieved.

Immediately after the steady state was reached, an XPS analysis was performed on the ion-beam-induced samples with a takeoff angle of 35° in order to maximize the signal from the surface. The results derived from the Si $2p$ photoelectron region are shown in Fig. 4, where the relative concentration of Si chemical states is plotted as a function of the angle of incidence after the steady state is reached.

The valence band of the altered layers experiences a strong increase in total width from 11 eV (crystalline Si) or 10 eV (SiO_2) to 15 eV. This effect arises primarily from the merging of the valence bands of Si and SiO_2 to one single wider band for these altered layers. The new altered valence band can be divided in two different regions. Peaks I, II, and III form the Si-like subband, while the IV, V, VI, VII, and VIII peaks form the SiO_2-like valence band (Fig. 5 shows the spectrum corresponding to the valence band for an altered layer bombarded at 35°).

As compared to the original bands (Si and SiO_2) no additional peaks appear in the spectrum. Instead of the symmetry labels used to describe peaks appearing in the crystalline Si valence band we use for the altered layer valence band a different notation (roman numbers), since long-range order or crystalline symmetry disappears after ion-beam-induced amorphization, despite the fact that the new valence bands can still be understood in terms of a molecular orbital description.

Peaks I, II, and III correspond solely to the L_3, X_4, and $W_2+\Sigma_{1\,\min}$ bands that were described as the first region in the crystalline-Si valence band and they are understood as Si $3p$-like orbitals corresponding to the pres-

TABLE II. Energies (eV) for the different features of the valence band of SiO_2 experimentally determined by XPS (±0.3 eV), compared to the results of Fischer *et al.* and using calculations of Tossel *et al.* All energies are referenced to the top of the valence band (see Fig. 3).

Tossel calc.[a]	XPS expt.	Fischer expt.[b]
$1e_{(I)}+5t_{2(I)}$	2.3	2.0
$1t_{1(I)}$	4.2	3.5
V	5.7	5.4
$4t_{2(II)}$	7.3	6.5
$5a_{1'(II)}$	8.9	9.0
$5a_{1(II)}$	10.2	10.0

[a]References 46 and 47.
[b]Reference 35.

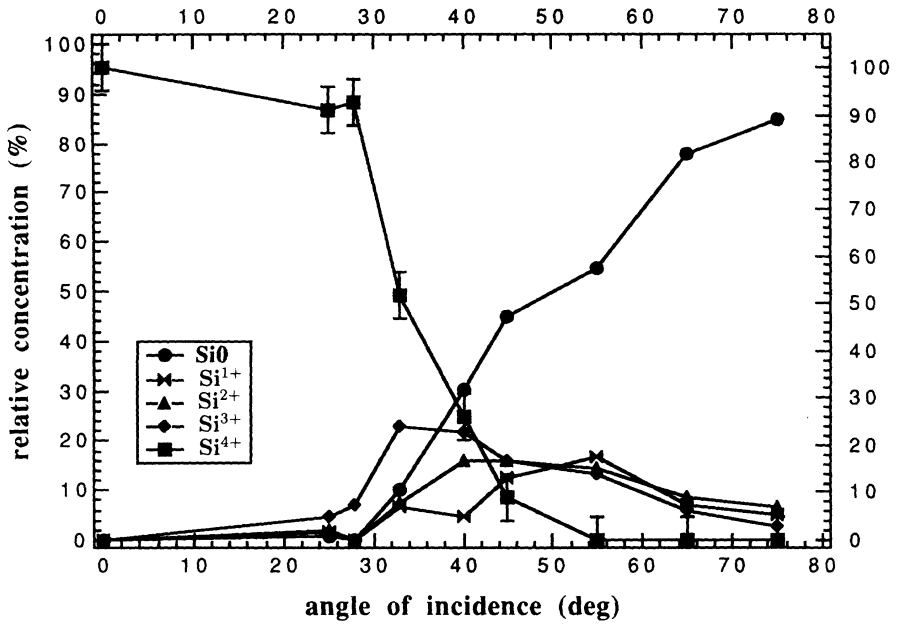

FIG. 4. Si chemical state relative concentration as a function of the angle of incidence derived from the Si 2*p* photoelectron peak after 5-keV O_2^+ bombardment.

ence of Si-Si bonds in a highly damaged Si matrix. Peaks IV and V account for nonbonding O 2*p*-like molecular orbitals, as already found in the case of SiO_2 ($1e+5t_2$ and $1t_1$), with a small influence of the L_1 and L_2 peaks (*s*-*p* hybrids) that are present in the Si valence band at this energy position.

The deep valley *V* determined for SiO_2 is now partially overlapped by the L_2 peak arising from Si-Si interactions. Peaks VI, VII, and VIII correspond to oxide bonding orbitals between Si and O and only peak VI becomes affected by the presence of the Γ_1 peak (*s*-like orbitals) of Si-Si interaction origin.

In Fig. 6, a comparison between the valence bands for crystalline Si, altered layers formed at 35°, 30°, 25°, 15°, and 0° and thermally grown SiO_2 is shown. The zero energy for all figures has been defined at the top of the valence band of SiO_2.

The description of the valence band for the altered layer, in terms of a mixture of the Si and the SiO_2 bands, is supported by the consistency of the energy position of the different peaks (Fig. 7) and the change of their relative ratios (Fig. 8) with increasing oxidation.

The three peaks corresponding to Si-Si (I, II, and III) maintain the same energy position as compared to Si, whereby the Si-Si 3*p*-like orbitals remain unchanged after ion-beam-induced oxidation The relative variations of these Si valence-band features such as peaks I, II, and III should be understood as a measure of the induced suboxidation in the altered layer, since the suboxide molecules include one silicon atom bond to one (Si^{1+}), two (Si^{2+}), and three (Si^{3+}) oxygen atoms and three, two, and one silicon atoms (Si 3*p*-like orbitals), respectively. The intensity of peaks I, II, and III decreases with decreasing angle of incidence or, put differently, with increasing degree of oxidation.

It is, however, quite surprising that at a low angle of incidence (15°) or normal incidence (0°), peak II and III still show up, although the intensity is very low. In both cases, however, peak I is not present, giving rise to an increase of band gap for these altered layers which are becoming more and more oxidelike structures.

It is important to note that at normal incidence (corresponding to 100% oxidation according to the Si 2*p* photoelectron peak deconvolution) peaks II and III are still present. This can be explained as a result of ion-induced damage of the built-up SiO_2 layer,[44] resulting in an al-

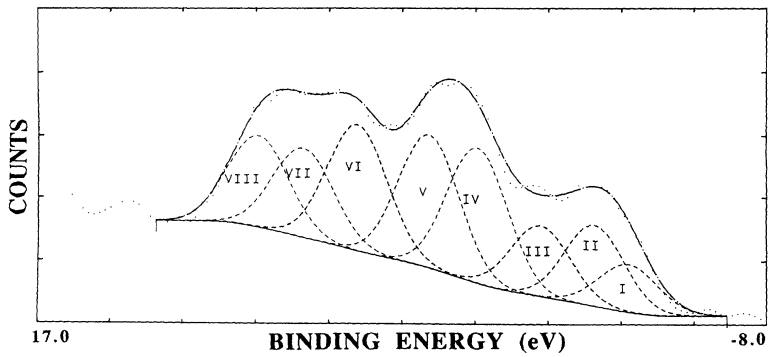

FIG. 5. XPS spectrum for the valence band of the altered layer formed after a 5-keV/35° O_2^+ bombardment of Si.

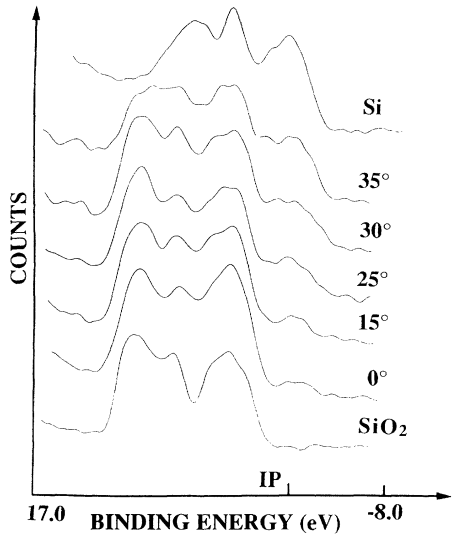

FIG. 6. XPS spectra for the valence bands (from top to bottom) of Si, altered layers formed with an angle of incidence of 35°, 30°, 25°, 15°, 0°, and SiO_2.

tered layer with some molecules formed by three oxygen atoms bonded to one Si atom. The fourth oxygen atom necessary to form the SiO_2 molecule, is sputtered by the ion beam leaving an unpaired *p*-like orbital (based on its binding energy) with similar characteristics as a Si 3*p*-like orbital peak. This peak is measured in region I of the valence band but cannot be seen in the Si 2*p* photoelectron region. Indeed the chemical environment of the Si 2*p* core level in this molecule is comparable to a SiO_2 environment, and, therefore, no chemically induced shift is present or it is too low to be measured with our energy resolution. If the unsaturated bond is located on the surface, it could react with water vapor to form a Si-OH–Si-H termination,[33] which would give rise to a peak in the Si 2*p* region too small to be detected.

The peaks corresponding to the nonbonding O 2*p* orbitals (IV and V) remain, regardless of the angle of incidence, in a ratio of about 1:1 as in the SiO_2 case. The energy position of these peaks is constant and in good agreement with the corresponding SiO_2 peaks.

For peaks VI and VIII we measure a very similar dependence with the angle of incidence, i.e., an increase in intensity with increasing degree of oxidation, which confirms the link between these peaks with the bonding orbitals Si-O. At 100% oxidation, peaks VI and VIII do not reach the SiO_2 intensity, probably due to the induced damage as already pointed out for peaks II and III. The intermediate peak VII decreases with decreasing angle of incidence in contrast with the other bonding orbitals. This decrease must be seen as a lowering of the contribution of Si-Si s-s–like orbitals, but not as a lowering of the bonding orbitals (Si-O). The contribution of this peak is still important at an angle of incidence of 35°.

Finally, a summary of the evolution of each peak present in the valence band of the altered layers is presented in Table III. The following valence-band features are shown: (a) the electron interactions responsible for the peaks, (b) observed peaks in the valence band spectrum of thermally grown SiO_2, (c) peaks in the valence-band spectrum of the altered layer bombarded at normal incidence, and (d) the evolution of the peak area with increasing degree of oxidation [indicated by the arrow: increase (up) or decrease (down)].

B. Model for the Si^+-ion emission during sputtering

Wittmaack and von Criegern[52–55] measured the variation of the Si^+ yield as a function of the angle of incidence. Whereas Wittmaack used a rotation in a plane parallel with the quadrupole, von Criegern was tilting around an axis perpendicular to the quadrupole. Although for the ion-solid interaction both rotations are identical, they are not with respect to the secondary ion detection system. In particular in the case of von

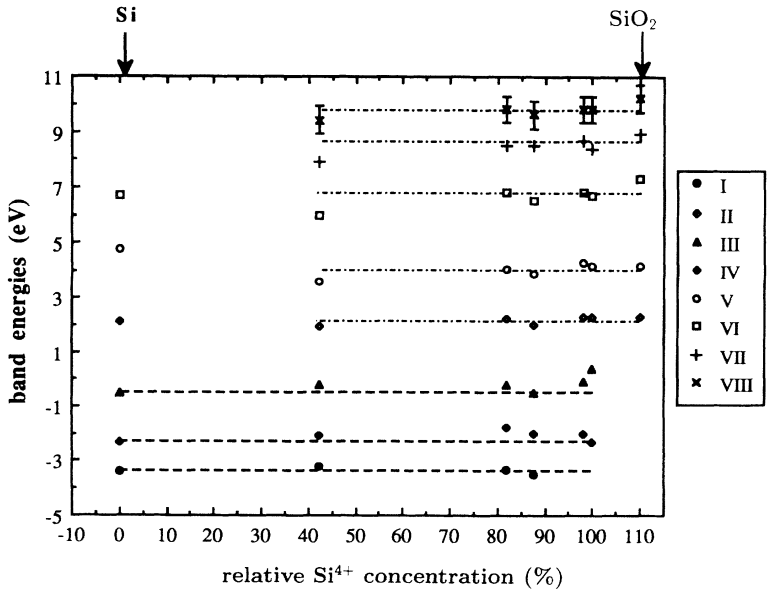

FIG. 7. Energy position (referred to the top of the SiO_2 valence band) for the different bands as a function of Si^{4+} chemical state relative concentration (or the angle of incidence) as derived from the Si 2*p* photoelectron peak. Si and SiO_2 labels mark the peak position for crystalline Si (dashed line) and thermal SiO_2 (dashed-point line). The assignment of the peaks is explained in the text.

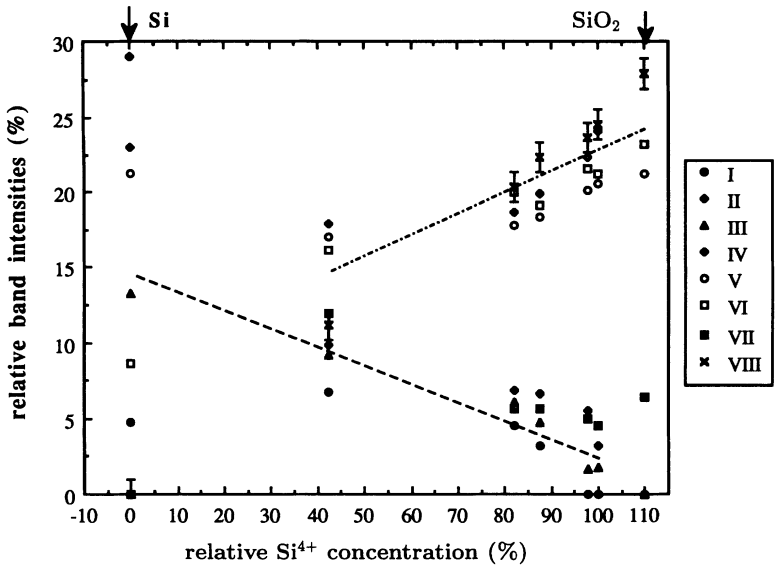

FIG. 8. Relative intensities for valence-band peaks as a function of the Si^{4+} relative concentration (or angle of incidence) as derived from the Si 2*p* photoelectron peak. The relative intensities for crystalline Si and thermal SiO_2 are also shown. The dashed and the dash-dotted lines mark the evolution of the Si-like and SiO_2-like band features, respectively.

Criegern, the collection and transmission efficiency of the secondary ion is changing with tilt angle. The results can be corrected for this effect by performing a similar experiment using inert-gas bombardment. In this case, no chemical effects on the secondary ion yields are present and one can attribute any changes in secondary ion yield to changes in collection and transmission efficiency. Assuming that those changes are very similar for oxygen and inert-gas bombardment, one can correct the Si^+-yield curve recorded with oxygen bombardment, by dividing that with the Si^+-yield curve under inert-gas bombardment. Although the magnitude of the correction in the case of von Criegern and Wittmaack is drastically different, the application of this correction procedure leads to very similar results (Fig. 9). Both curves show a slow decrease in Si^+ yield when going from 0° to 30°, followed by a very rapid decline for higher angles. Especially in this region some differences between both curves can be seen. One of the reasons could be that one is dealing with relatively small signals such that the accuracy gradually decays. In order to overcome this problem we have taken the average between both as the Si^+ secondary ion yield in the remaining part of the paper.

In order to test the need for the resonant tunneling model, let us first try to relate the change in ionization yield (or secondary ion intensity) as a function of the angle of incidence,[54,55] with the amount of Si^{4+} or total O concentration on the surface (Figs. 10 and 11). (We recall that in Fig. 10, as well as in Fig. 11, a secondary ion yield corresponding to 10-keV O_2^+ ion energy was used but, owing to the very small energy dependence in this region, the yield for 5-keV O_2^+ ion energy will be nearly identical.[54,55] A linear enhancement of the Si^+ secondary

TABLE III. The most important features [electronic interaction, peak present in thermal SiO_2, peaks in the ion-beam-oxidized (IBO) sample at 0°, and peak area evolution when increasing the degree of oxidation (oxid.)] for each of the eight peaks measured in the valence band of the different altered layers.

Peak	Electronic interaction assignment	Thermal SiO_2	IBO	Peak evolution 0° increasing oxid.
I	Si3*p*-3*p*	No	No	⇓
II	Si3*p*-3*p*	No	Yes	⇓
III	Si3*p*-3*p*	No	Yes	⇓
IV	O2*p*-2*p*	Yes	Yes	⇑
V	O2*p*-O2*p*	Yes	Yes	⇑
VI	O2*p*-Si3*s* + 3*p*	Yes	Yes	⇑
VII	(O2*p*-Si3*s* + 3*p*)/(Si3*s*-3*s*)	Yes	yes	⇓
VIII	O2*p*-Si3*s* + 3*p*	Yes	Yes	⇑

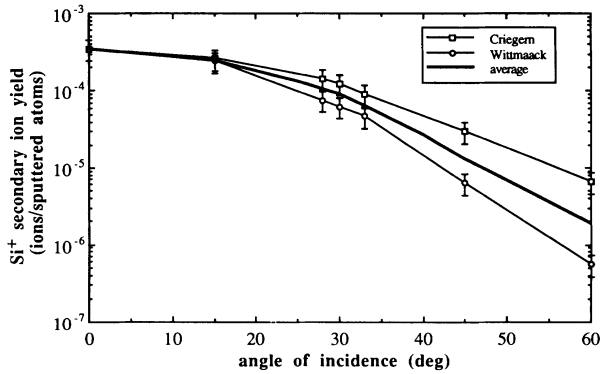

FIG. 9. Si^+ secondary ion yield (corrected for changes in collection and transmission effectivity) as a function of the angle of incidence as measured by von Criegern and Wittmaack (Refs. 52–55). The solid line is the average Si^+ secondary ion yield used in this paper.

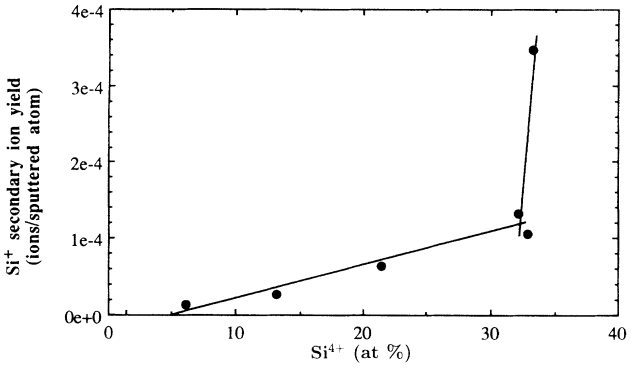

FIG. 10. Si^+ secondary ion yield as a function of Si^{4+} atomic concentration.

ion yield with respect to the Si^{4+} relative concentration can be found over nearly two orders of magnitude, suggesting that the increase in yield is closely related to the Si^{4+} bond formation. As shown in Fig. 11, a power-law dependence of the yield on the total oxygen concentration is found for concentrations up to 65 at. %, as has already been observed previously.[19,54,55] The linear dependence on the Si^{4+} bond concentration is a clear indication of the local bond breaking model for ionization as discussed by Yu.[17] (Note that in the treatment of local bond breaking, one does not necessarily expects a linear dependence. For instance, Oechsner and Sroubek[5] suggest an enhancement factor R in ionization for the first energy suboxide state Si^{1+}, R^2 for the Si^{2+}, R^3 for the Si^{3+}, and R^4 for the Si^{4+}.) It is, however, necessary to point out that at relative concentrations higher than 30 at. % a steplike increase in the yield takes place. For oxygen concentrations higher than 65 at. % this steplike increase in the Si^+ secondary ion yield is once again observed. Hence in this region the direct correlation between an increase in oxide bonds and the degree of oxidation is lost, invalidating the local-bond-breaking model here.

The steplike increase for very high Si^{4+} concentrations might be correlated with the formation of a "complete" SiO_2 layer on the surface. A possible explanation could be that the transition to a complete SiO_2 layer also induces a drastic change in band-gap structure. Also, Yu

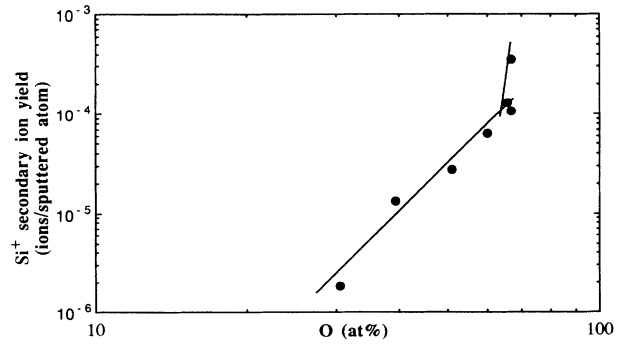

FIG. 11. Si^+ secondary ion yield as a function of total O concentration.

using oxygen adsorption observed that it is possible to increase the Si^+ yield for the same oxygen coverage, solely by heating the sample, which according to his observations improved the bond structure of the formed oxide.

The influence of the band structure on the secondary ion yields suggests that one has to consider an additional mechanism for secondary ion emission such as the tunneling effect described by Yu.

The results obtained in the previous section indicate that the valence band of the altered layer can be described by a mixture of Si and SiO_2. The most surprising feature is the presence of occupied states in the region corresponding to peaks I, II, and III for angles smaller than 30°, where the Si $2p$ spectrum indicates complete or partial oxidation but always without the presence of the pure Si chemical state. The results indicate that the density of states in this region is correlated with the angle of incidence, suggesting an effect of these states on the SIMS yield.

The obvious framework to include this contribution is the resonant tunneling model. Before doing this, it is important to realize that presently the model was only formulated for metals where the Fermi level defines the energy region with occupied states. For a semiconductor like Si, or an insulator like SiO_2, we must substitute the Fermi level by the top of the valence band and take into account the fact that only a limited number of occupied states are present in this energy region.

These assumptions, in the case of SiO_2, imply that the first ionization energy for Si in the free space (I_p) needs to be referenced to the top of the valence band of thermal SiO_2 (2.1 instead of 8.1 eV that refers to the vacuum level, since the energy distance from the SiO_2 top of the valence band to the vacuum level is 10.2 eV)[32] and that there will be no possibility for tunneling, since the first ionization level for Si in the free space (I_p) lies in the band gap and no occupied electron states are available at that level. However, in the case of crystalline Si and the altered layers (at all angles of incidence) the Si (I_p) level lies in the region formed by peaks I, II, and III of their respective valence band, in which case the tunneling effect is possible, since the density of states at that energy is not zero. The relative position for the first ionization level of Si in free space (I_p) with respect to the several valence-band XPS spectra is shown in Fig. 6.

To quantify the tunneling effect in the case of Si, we have derived from Eq. (1) an expression for the relative variation of the probability of tunneling transitions between loosely bond electronic states (on the top of the valence band) and the i_p level for the sputtered Si^+ atom (normalized to the tunneling probability in the pure Si case)

$$P_{\mathrm{rt}}=\frac{\int_{\infty}^{i_p} n(E)\{1-\exp[-(I_p-E)]/\varepsilon_0\}dE}{\int_{\infty}^{i_p} n_{\mathrm{Si}}(E)\{1-\exp[-(I_p-E)]/\varepsilon_0\}dE}, \quad (2)$$

where $n(E)$ is the XPS signal at an energy E proportional to the density of states of energy E in the valence band. $n(E)$ is a function that can be derived from the XPS valence-band measurements. The calculations have been

carried out with $\varepsilon_0 = 1.0$ eV, since available measurements[12] have shown that for similar experimental conditions ε_0 can vary between 0.3 and 1.3 eV. The results presented in this paper do not change significantly while using values of ε_0 in the mentioned range.

The function $\{n(E)(1-\exp[-I_p-E)])\}$ is represented in Fig. 12. It has been derived from the XPS valence-band data for crystalline Si and the altered layers obtained at 35°, 30°, 25°, 15°, and 0° angles of incidence. We need to integrate expression (1), which was calculated for transitions between two single occupied states separated by a potential barrier,[9-11] from the energy value corresponding to the top of the valence band to the value of i_p (free space) $=I_p$, since all over this energy range the valence band presents occupied states that may transit to the varying energy level (i_p) in the sputtered ion.

One can observe pronounced differences in the shape of this function when going from crystalline Si to normal incidence bombardment (SiO_2 formation). Qualitatively, one can explain the distributions for 0° and 15°, by realizing that nearly perfect SiO_2 is formed, which has a wider band gap causing the distribution to break off at lower energies.

The function must be zero for $(I_p-E)<0$ since this implies $E>I_p$. As the tunneling occurs towards the instantaneous ionization level $I_p(z)$, this would imply $i_p(z)>I_p$ which is of course impossible. On the other hand, for (I_p-E) large, the probability of tunneling is zero. In fact, this condition implies that E is very small, and hence the level $i_p(z)$ to which tunneling occurs will also be very small. In that case, $i_p(z)$ will be located high within the band gap and no electronic levels are available for tunneling. The respective function for SiO_2 is zero for all energies, since the ionization level in the free space I_p lies above the top of its valence band.

From this function we can calculate P_{rt} [Eq. (2)], which gives a value for the importance of tunneling effect as a function of the angle of incidence (Fig. 13). For angles larger than 35° the tunneling probability is practically the same magnitude as for crystalline Si, whereas for

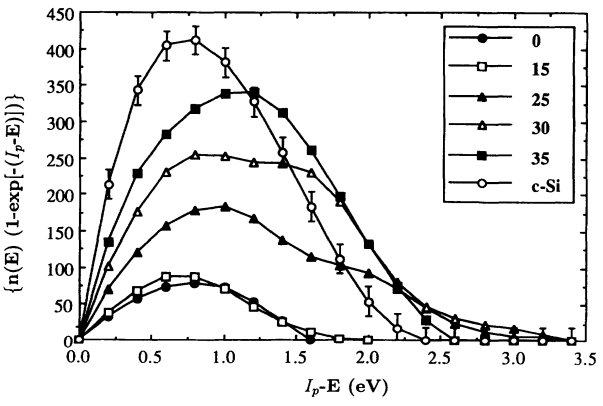

FIG. 12. Function $\{n(E)(1-\exp[-(I_p-E)])\}$ [where $n(E)$ is derived from the XPS valence-band data] as a function of the energy distance I_p-E for various angles of incidence (as shown in the inset) and crystalline Si.

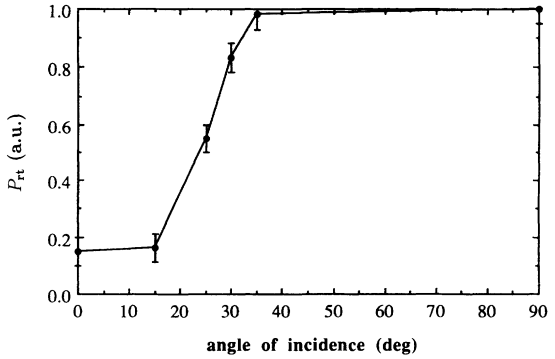

FIG. 13. P_{rt} as a function of the angle of incidence and for the case of crystalline Si.

angles smaller than 35° a strong decrease of the tunneling effect is observed since the valence band undergoes large variations in region I.

So far we have discussed the XPS results in terms of the probability of the tunneling effect, but in terms of the probability for secondary ion emission and the correlation with the SIMS yields, the complementary function of Fig. 14 should be used. It is clear that for large angles of incidence (>30°–35°) the tunneling effect is less significant for secondary ion emission, and the local-bond-breaking mechanism will be dominant, whilst for low angles of incidence where the degree of oxidation, and hence the chemical enhancement varies very little, the strong variation in the tunneling effect is the main factor influencing the SIMS yield. This becomes more evident if we look at Fig. 15, which shows the evolution of the Si^+ secondary ion yield as a function of the relative tunneling probability variation (P_{rt}). A linear dependence of the Si^+ signal with P_{rt} is found for angles of incidence lower than 30°–35°, whereas, for larger angles of incidence, the effect is negligible and the secondary ion yield is determined by the local bond structure.

The results can be summarized as follows:

(a) At angles of incidence larger than 30°–35°, the silicon is gradually converted to an oxide-rich layer with, however, properties (as derived from the valence band) that are still crystalline-siliconlike. Hence no variations in tunneling (neutralization) probability can be detected

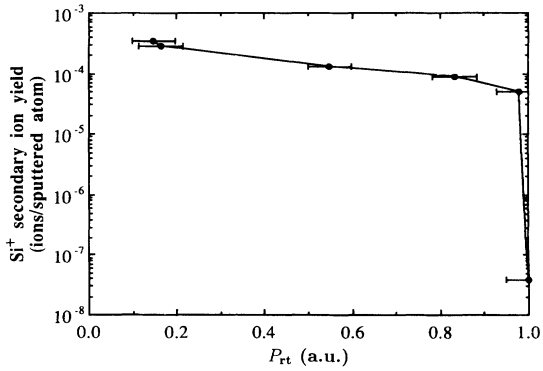

FIG. 14. Si^+ secondary ion yield as a function of the P_{rt} function.

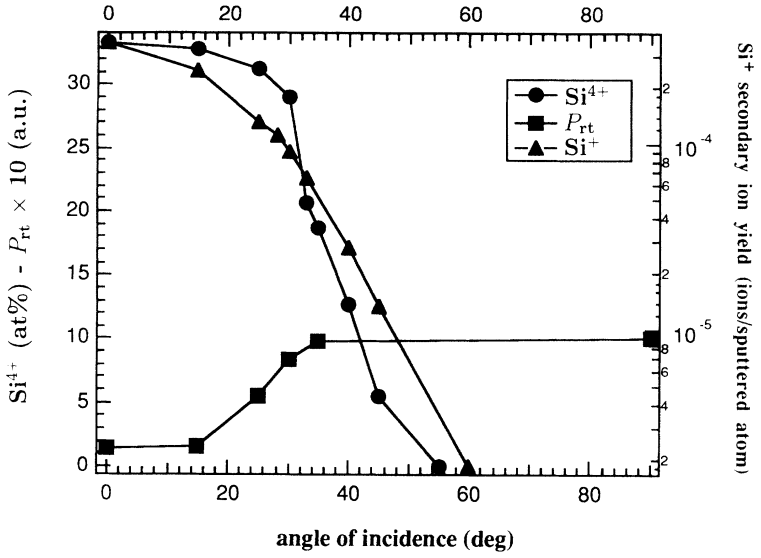

FIG. 15. Comparison between the evolution of the Si^{4+} atomic concentration, the Si^{+} ion emission, and the relative probability (multiplied by a factor of 10) with the angle of incidence.

and the secondary ion emission is dominated by the increase in local Si-O bonds.

(b) At angles smaller than 30°–35°, the silicon surface becomes more and more oxidelike. The increased oxidation gives rise to dramatic changes in the valence-band structure leading to variations in tunneling probability. As the surface is always nearly completely oxidized (80–100%), very little variation in chemical enhancement is expected. Basically, we now have a high emission rate of secondary ions (due to the large number of Si-O bonds) and a reduced tunneling probability (in going to 0°) due to the changes in the valence band, leading to an increase in detected secondary ion signals.

The angular dependences of electron tunneling probability, Si^{4+} relative concentration, and the SIMS yield are given in Fig. 15. It is clear that any changes in the SIMS yield can be correlated either with changes in tunneling probability or with changes in local bonds.

IV. CONCLUSIONS

The different degree of oxidation in the surface of the altered layer gives rise to variations in the Si^{+} ion emission during SIMS measurements. Two rather different regimes can be observed for the evolution of the Si^{+} ion emission as a function of the oxygen incorporation. In this work, a special interest on the analysis and interpretation of the valence-band region was made. A comparison with the experimentally measured and theoretically derived Si valence band and SiO_2 valence band suggests that the "new" valence bands for the altered layers are formed by a combination of those two. This arises from the fact that Si-Si bonds are present in the silicon suboxide molecules and, therefore, the corresponding $3p$-$3p$ Si-like subband, which extends towards the silicon Fermi level, forms the top of the respective new valence bands. Small variations in intensity and energy position for this subband have dramatic implications on the intensity of the Si^{+} ion emission during sputtering in SIMS measurements.

A correlation between the valence-band variations and the two presently existing atomic models for ion emission has been derived, and a model combining chemically enhanced emission and resonant tunneling effect has been proposed to explain the variations in ion emission during oxygen bombardment for Si targets.

[1]M. L. Yu and N. D. Lang, Phys. Rev. Lett. **50**, 127 (1983).
[2]K. Franzreb, A. Wucher, and H. Oechsner, Phys. Rev. B **43**, 14 396 (1991).
[3]P. Williams, in *Secondary Ion Mass Spectrometry, SIMS VII*, edited by A. Benninghoven, C. A. Evans, K. D. Mckeegan, H. A. Storms, and H. W. Werner (Wiley, New York, 1990), p. 15.
[4]M. L. Yu and N. D. Lang, Nucl. Instrum. Methods Phys. Res. Sect. B **14**, 403 (1986).
[5]H. Oechsner and Z. Sroubek, Surf. Sci. **127**, 10 (1983).
[6]M. L. Yu and K. Mann, Phys. Rev. Lett. **57**, 1476 (1986).
[7]Z. Sroubek, in *Secondary Ion Mass Spectrometry, SIMS VI*, edited by A. Benninghoven, A. M. Huber, and H. W. Werner (Wiley, New York, 1988), p. 17.
[8]M. L. Yu, in *Secondary Ion Mass Spectrometry, SIMS VI* (Ref. 7), p. 41.
[9]N. D. Lang and A. R. Williams, Phys. Rev. B **18**, 616 (1978).
[10]J. K. Nørskov and B. I. Lundqvist, Phys. Rev. B **19**, 5661 (1979).
[11]N. D. Lang, Phys. Rev. B **27**, 2019 (1983).
[12]M. L. Yu, Phys. Rev. Lett. **47**, 1325 (1981).
[13]L. Landau, Phys. Z. Sowjetunion **2**, 46 (1932).
[14]C. Zener, Proc. R. Soc. London Ser. A **137**, 696 (1932).
[15]E. C. Stueckelberg, Helv. Phys. Acta **5**, 369 (1932).
[16]C. Coudray and G. Slodzian, *Secondary Ion Mass Spectrometry, SIMS VI* (Ref. 7), p. 45.
[17]M. L. Yu, Nucl. Instrum. Methods Phys. Res. Sect. B **15**, 151 (1986).

[18]W. Reuter, Nucl. Instrum. Methods Phys. Rev. Sect. B **15**, 176 (1986).
[19]K. Wittmaack, Surf. Sci. **112**, 168 (1981).
[20]P. J. Grunthaner, M. H. Hecht, F. J. Grunthaner, and N. M. Johnson, J. Appl. Phys. **61**, 629 (1987).
[21]M. L. Cohen and J. R. Chelikowsky, in *Handbook on Semiconductors,* edited by T. S. Moss (North-Holland, Amsterdam, 1982), Chap. 4b, p. 219.
[22]M. L. Cohen and J. R. Chelikowsky, *Electronic Structure and Optical Properties of Semiconductors,* 2nd ed., Springer Series in Solid-State Sciences Vol. 75 (Springer-Verlag, Berlin, 1989).
[23]L. Ley, S. Kowalczyk, R. Pollak, and D. A. Shirley, Phys. Rev. Lett. **29**, 1088 (1972).
[24]M. L. Cohen and J. D. Joannopoulos (private communication).
[25]D. J. Stukel, T. C. Collins, and R. N. Euwema, in *Electronic Density of States, Proceedings of the Third International Materials Research Symposium,* edited by L. H. Bennett, Natl. Bur. Stand. Spec. Publ. No. 323 (U.S. GPO, Washington, DC, 1971).
[26]R. A. Pollak, L. Ley, S. Kowalczyk, D. A. Shirley, J. D. Joannopoulos, D. J. Chadi, and M. L. Cohen, Phys. Rev. Lett. **29**, 1103 (1972).
[27]D. E. Eastman, W. D. Grobman, J. L. Freeouf, and M. Erbudak, Phys. Rev. B **9**, 3473 (1974).
[28]G. Hollinger and F. J. Himpsel, J. Vac. Sci. Technol. A **1**, 640 (1983).
[29]J. Tersoff and D. R. Hamann, Phys. Rev. B **28**, 1168 (1983).
[30]J. Robertson, J. Phys. C **18**, 947 (1985).
[31]P. S. Ho and G. W. Rubloff, Thin Solid Films **89**, 433 (1982).
[32]H. Ibach and J. E. Rowe, Phys. Rev. B **10**, 710 (1974).
[33]G. W. Rubloff, Phys. Rev. B **25**, 4307 (1982).
[34]L. Ley, R. A. Pollak, F. R. McFeely, S. P. Kowalczyk, and D. A. Shirley, Phys. Rev. B **9**, 600 (1974).
[35]B. Fischer, R. A. Pollak, T. H. DiStefano, and W. D. Grobman, Phys. Rev. B **15**, 3193 (1977).
[36]T. H. DiStefano and D. E. Eastman, Phys. Rev. Lett. **27**, 1560 (1971).
[37]S. Ciraci and S. Ellialtioglu, Solid State Commun. **40**, 587 (1981).
[38]A. Balzarotti and A. Bianconi, Phys. Status Solidi B **76**, 689 (1976).
[39]R. B. Laughlin, J. D. Joannopoulos, and D. J. Chadi, Phys. Rev. B **21**, 5733 (1980).
[40]M. H. Reilly, J. Phys. Chem. Solids **31**, 1041 (1970).
[41]S. Ciraci and I. P. Batra, Phys. Rev. B **28**, 982 (1983).
[42]R. B. Laughlin, Phys. Rev. B **22**, 3031 (1980).
[43]S. P. Kowalczyk, F. R. McFeely, L. Ley, V. T. Gritsyna, and D. A. Shirley, Solid State Commun. **23**, 161 (1977).
[44]V. M. Bermudez and V. Ritz, Phys. Rev. B **20**, 3446 (1979).
[45]J. Pollmann and S. T. Pantelides, Phys. Rev. B **18**, 5524 (1978).
[46]J. A. Tossell, D. J. Vaughan, and K. H. Johnson, Chem. Phys. Lett. **20**, 329 (1973).
[47]J. A. Tossell, J. Am. Chem. Soc. **97**, 4840 (1975).
[48]H. R. Philipp, Solid State Commun. **4**, 73 (1966).
[49]G. Klein and H. U. Chun, Phys. Status Solidi B **49**, 167 (1972).
[50]G. Wiech, in *Soft X-ray Band Spectra,* edited by D. J. Fabian (Academic, New York, 1968), p. 59.
[51]K. Lauger, dissertation, University of Munchen, 1960 (unpublished).
[52]R. v. Criegern and I. Weitzel, in *Secondary Ion Mass Spectrometry SIMS V,* edited by A. Benninghoven, R. J. Colton, D. S. Simons, and H. W. Werner (Springer, Berlin, 1986), p. 319.
[53]Y. Homma and K. Wittmaack, J. Appl. Phys. **65**, 5061 (1989).
[54]K. Wittmaack, Nucl. Instrum. Methods Phys. Res. **218**, 307 (1983).
[55]K. Wittmaack, Nucl. Instrum. Methods Phys. Res. Sect. B **2**, 674 (1984).